11

Optical and optoelectronic properties of oxidized borophene and oxidized borophene based van der Waals heterostructures

© M.M. Slepchenkov[1], D.A. Kolosov[1], O.E. Glukhova[1,2]

[1] Saratov National Research State University,
410012 Saratov, Russia
[2] I.M. Sechenov First Moscow State Medical University,
119991 Moscow, Russia

e-mail: slepchenkovm@mail.ru

Received December 27, 2023
Revised January 15, 2024
Accepted March 05, 2024

In this paper, we used to carry out a predictive analysis of the possibility of controlling the optical and optoelectronic properties of van der Waals quasi-2D heterostructures formed by buckled triangular borophene and monolayers of graphene-like gallium nitride GaN and zinc oxide ZnO, due to the functionalization of borophene with oxygen. The appearance of an energy gap in the band structure of the studied borophene/GaN and borophene/ZnO van der Waals heterostructures, caused by the presence of a gap between the valence band and the conduction band in the electronic structure of oxidized (O-) borophene, is discovered. It is shown that in the case of light polarization in the direction perpendicular to the zigzag edge of the borophene atomic lattice, a peak with an intensity of about 30% appears in the visible range of the absorption spectrum of heterostructures based on O-borophene and GaN/ZnO monolayers. At the same time, for heterostructures with pure borophene, the absorption value in the visible range was no more than 5−10%. It is revealed that the profiles of the photocurrent spectrum of O-borophene/GaN and O-borophene/ZnO heterostructures have a similar shape to the spectra of O-borophene. It is predicted that O-borophene/GaN and O-borophene/ZnO heterostructures may be promising as sensitive elements of solar cells operating both on the Earth's surface and beyond.

Keywords: density functional theory, absorption coefficient, photocurrent spectrum, light polarization, photovoltaics.

DOI: 10.61011/EOS.2024.03.58741.33-24

Introduction

The discovery of graphene and other 2D materials with unique physical properties has caused a noticeable surge of interest from researchers working in materials science, condensed matter physics, and nano- and optoelectronics [1]. The family of 2D materials has already grown quite large and includes 2D carbon materials [2]; chalcogenides and dichalcogenides of transition metals [3,4]; carbides, nitrides, and carbonitrides of transition metals (MXenes) [5]; perovskites [6]; metal oxides [7]; and magnetic materials and their derivatives [8]. Vertical stacking of monolayers of 2D materials with different electronic, optical, and magnetic properties provides an opportunity to fabricate heterostructures of two or more layers with distinct physical properties that differ from the properties of individual monolayers [9–12]. Since weak van der Waals forces are the only ones acting between monolayers, one may combine 2D structures with different lattice parameters and types of crystal structure. Such experimental techniques as alignment transfer, mechanical exfoliation, liquid-phase exfoliation, vapor-phase deposition, and layer-by-layer electrostatic self-assembly are used to fabricate van der Waals 2D heterostructures [13].

Diverse properties of van der Waals 2D heterostructures open up wide opportunities for development of various types of devices [14–20]. In particular, these heterostructures are used to fabricate vertical field-effect transistors [17]. The capacity for low-power operation and better performance due to a lower contact resistance are the advantages of tunnel field-effect transistors based on vertical heterostructures over conventional silicon transistors [17]. The anisotropy of electronic and optical properties of 2D materials and the potential to alter the band gap of these materials by adjusting their thickness allow one to design photodetectors with ultra-high sensitivity, ultrafast response, and high sensitivity to light polarization (especially in the infrared range) based on van der Waals heterostructures [18,19]. The use of layer-by-layer antiferromagnetic ordering in an atomically thin crystal makes these heterostructures suitable for magnetic data storage devices [20].

The synthesis of borophene and subsequent extensive studies of its properties set the stage for the design of van der Waals heterostructures based on this material. Borophene has many attractive properties, which include strength and flexibility, high thermal and electrical conductivity, and optical transparency [21]. Graphene–borophene [22] and borophene/organic van der Waals

heterostructures [23] have already been produced in experiments. Along with experimental studies of van der Waals heterostructures based on borophene, predictive *ab initio* studies, which are aimed at finding new combinations of borophene with other 2D materials for the production of van der Waals heterostructures for nano- and optoelectronics applications, are developing rapidly. Using the tight binding method and the nonequilibrium Green's functions formalism, the authors of [24] have performed predictive modeling to construct a model of a field-effect transistor based on a vertical graphene–boron nitride–borophene heterostructure. In the last few years, *in silico* studies into the prospects of application of borophene van der Waals heterostructures to implement a metal–semiconductor contact with a Schottky barrier have been carried out [25–27].

The objects examined in the present study are van der Waals heterostructures based on buckled triangular borophene, which features metallic conductivity, in combination with semiconductor monolayers of graphene-like gallium nitride GaN and zinc oxide ZnO. We have predicted the existence of these heterostructures by *ab initio* methods in [28]. The aim of the present study is to analyze, based on the results of *ab initio* calculations, the feasibility of controlled adjustment of the optical and optoelectronic properties of van der Waals borophene/GaN and borophene/ZnO heterostructures through functionalization with oxygen and to evaluate their potential for application in photovoltaics.

Research methods

The *ab initio* study was carried out using density functional theory (DFT) in the generalized gradient approximation (GGA) with the Perdew–Burke–Ernzerhof (PBE) functional [29] in the SIESTA package [30]. Van der Waals forces acting between the heterostructure layers were taken into account by applying Grimme's dispersion corrections [31]. The atomic structure of supercells of van der Waals heterostructures was optimized by minimizing the total energy using the Broyden–Pulay algorithm [32] and the DZP polarization functions basis set. The structure was relaxed until the change in force acting on each atom became less than 0.025 eV/Å. In order to exclude the mutual influence of heterostructure layers on each other in the nonperiodic direction (along axis Z), the vacuum gap was set to 20 Å. The cutoff energy was set to 150 Ry. The Brillouin zone was sampled by a $2 \times 6 \times 1$ Monkhorst–Pack [33] k-point grid. The LDA/GGA+U semi-empirical scheme in its modification proposed by Dudarev et al. [34] was used to solve the problem of underestimation of the band gap of the material.

Absorption coefficient A was calculated within the first-order non-stationary perturbation theory [35]:

$$A(\omega) = \frac{\omega}{cn(\omega)}\,\varepsilon_2(\omega), \tag{1}$$

where $\varepsilon_2(\omega)$ is the imaginary part of complex permittivity, $n(\omega)$ is the refraction index, c is the speed of light, and ω is the electromagnetic radiation frequency. Imaginary part of complex permittivity $\varepsilon_2(\omega)$ was determined by the following formula:

$$\varepsilon_2(\omega) = \frac{e^2}{\pi m^2 \omega^2} \sum_{v,c} \int_{\mathrm{BZ}} d\mathbf{k} \left| \langle \psi_{ck} | \hat{e}, \mathbf{p} | \psi_{vk} \rangle \right|^2 \times \delta(E_c(k) - E_v(k) - \hbar\omega), \tag{2}$$

where summation is performed over each pair of states of the valence (filled) and the conduction (unoccupied) bands and integration is carried out over all k-points in the Brillouin zone; indices c and v correspond to electronic states in the conduction and valence bands, respectively; and $E_{(c,v)}(k)$ and $\psi_{(c,v),k}$ are the energies and eigenfunctions of these states. The matrix element of the electronic dipole transition is between the occupied and unoccupied states, where $\hat{e}$ is the polarization vector and $\mathbf{p}$ is the momentum operator. Optical parameters of the examined van der Waals heterostructures were calculated for two different directions of light polarization (vector $\mathbf{E}$ parallel to axes X and Y) within the $0.2-2\,\mu$m wavelength range. Optical characteristics of the studied heterostructures were calculated with Brillouin zone sampling by a $114 \times 65 \times 1$ k-point grid.

A photocurrent spectrum was calculated based on the absorption spectrum. The maximum photocurrent was determined by the following formula:

$$I_{\max} = e \int_{\omega_1}^{\omega_2} \frac{a(\omega) Power_{\mathrm{solar}}(\omega)}{h\nu}\, d\omega, \tag{3}$$

where e is the electron charge, $a(\omega)$ is the absorption coefficient, $Power_{\mathrm{solar}}(\omega)$ is the solar radiation power, and $h\nu$ is the energy of a solar radiation quantum.

Atomic and electronic structure of supercells of van der Waals heterostructures based on oxidized borophene

We have already found the equilibrium atomic configurations of supercells of borophene/GaN and borophene/ZnO heterostructures via DFT calculations in [28]. In the present study, these configurations were modified by oxidizing borophene that is present in both heterostructures. The purpose of this modification was to open a gap in the band structure of borophene and heterostructures based on it to make them better suited for application in photovoltaic devices. The case of functionalization of the borophene surface with oxygen on one side of the monolayer with the formation of a „bridge" covalent bond (i.e., with one oxygen atom bound to two boron atoms) was considered. In was demonstrated in [36] through *ab initio* calculations that this configuration of oxidized borophene (O-borophene) features a band gap of ~ 0.2 eV. The feasibility of the

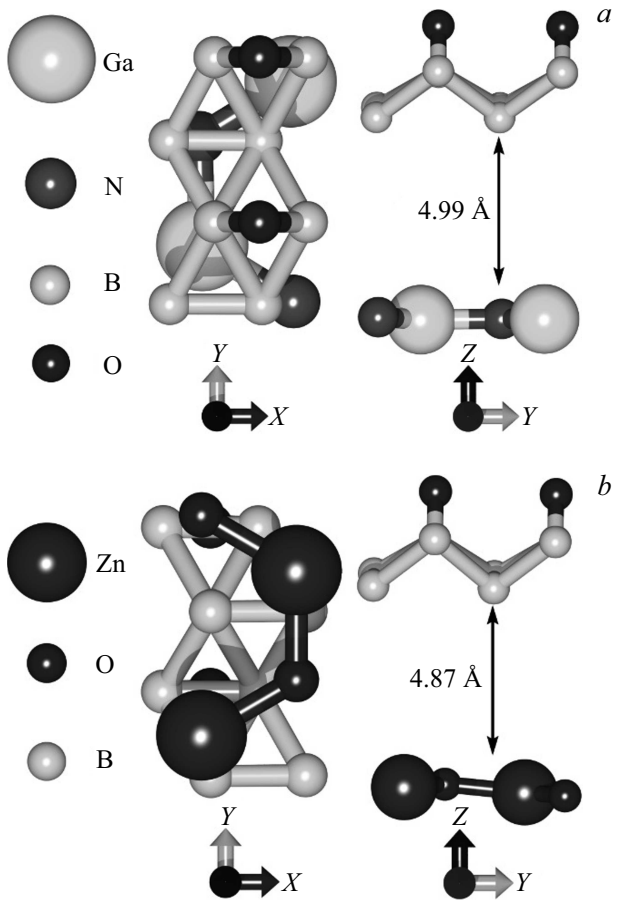

Figure 1. Atomic structure of supercells of van der Waals heterostructures based on oxidized borophene: *a* — borophene/GaN; *b* — borophene/ZnO.

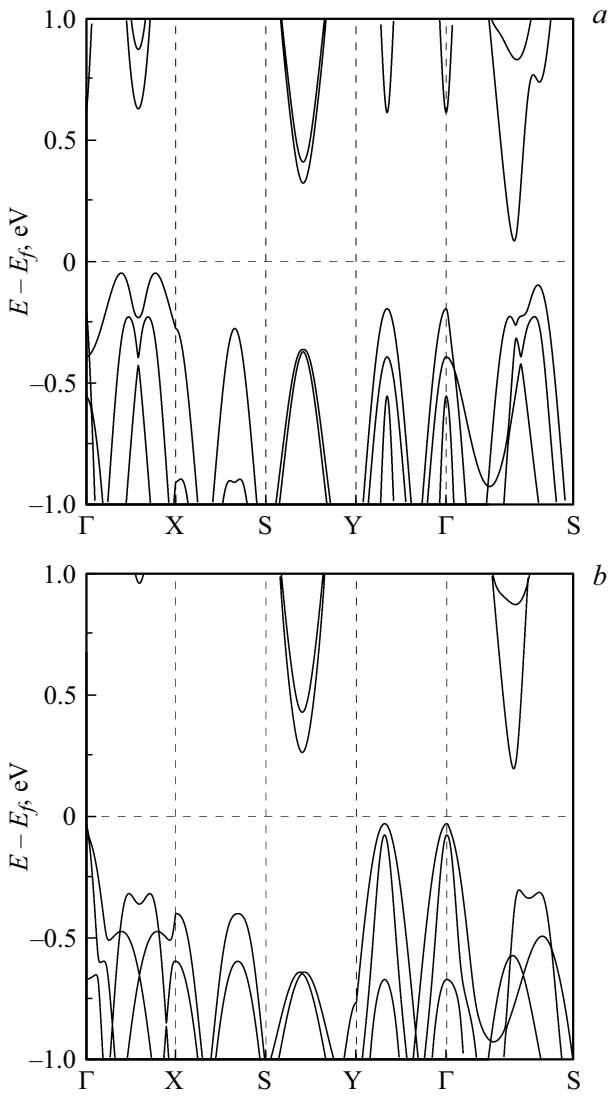

Figure 2. Fragments of the band structure near the Fermi level (shifted to 0 eV) of van der Waals heterostructures based on oxidized borophene: *a* — borophene/GaN; *b* — borophene/ZnO.

borophene oxidation procedure has also been demonstrated experimentally [37]. Figure 1 shows the equilibrium configurations of supercells of van der Waals quasi-2D heterostructures based on O-borophene and graphene-like GaN and ZnO. The translation vectors of the supercell of the O-borophene/GaN heterostructure along axes X and Y are $L_X = 3.41$ Å and $L_Y = 6.10$ Å respectively, and the distance between borophene and GaN monolayers is 4.99 Å. The translation vectors of the supercell of the O-borophene/ZnO heterostructure are $L_X = 3.339$ Å and $L_Y = 5.817$ Å, and the distance between O-borophene and ZnO monolayers is 4.87 Å.

Binding energy E_b was calculated to verify the thermodynamic stability of supercells of van der Waals O-borophene/GaN and O-borophene/ZnO heterostructures at room temperature. It was estimated as the difference between the total energy of the heterostructure and total energies of its constituent monolayers. The calculated binding energies E_b were -99 meV/atom for the O-borophene/GaN heterostructure and -192 meV/atom for the O-borophene/ZnO heterostructure. Negative values of the binding energy indicate that the structures are energetically stable; therefore, they may actually be fabricated.

The results of DFT calculations of the band structure of O-borophene confirmed the emergence of a band gap of ~ 0.22 eV that was reported in [36]. Fragments of the calculated band structures of supercells of van der Waals O-borophene/GaN and O-borophene/ZnO heterostructures are shown in Fig. 2. The Brillouin zone was a rectangle with the chosen $\Gamma{-}X{-}S{-}Y{-}\Gamma{-}S$ traversal trajectory. It can be seen that the electronic structure of both heterostructures features a gap between the valence band and the conduction band. The band gap width determined from the calculated band diagrams is 0.13 eV for the O-borophene/GaN heterostructure and 0.22 eV for the O-borophene/ZnO heterostructure.

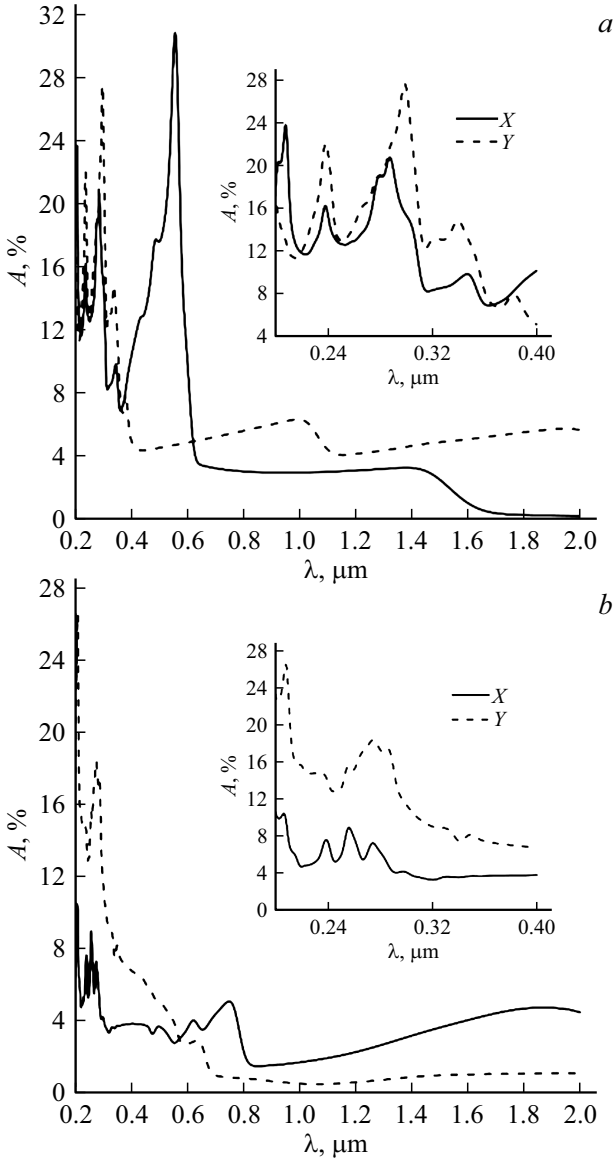

Figure 3. Optical absorption coefficient of the van der Waals borophene/GaN heterostructure with light polarized along the X (solid curves) and Y (dashed curves) axes: a — with oxidized borophene; b — with pure borophene.

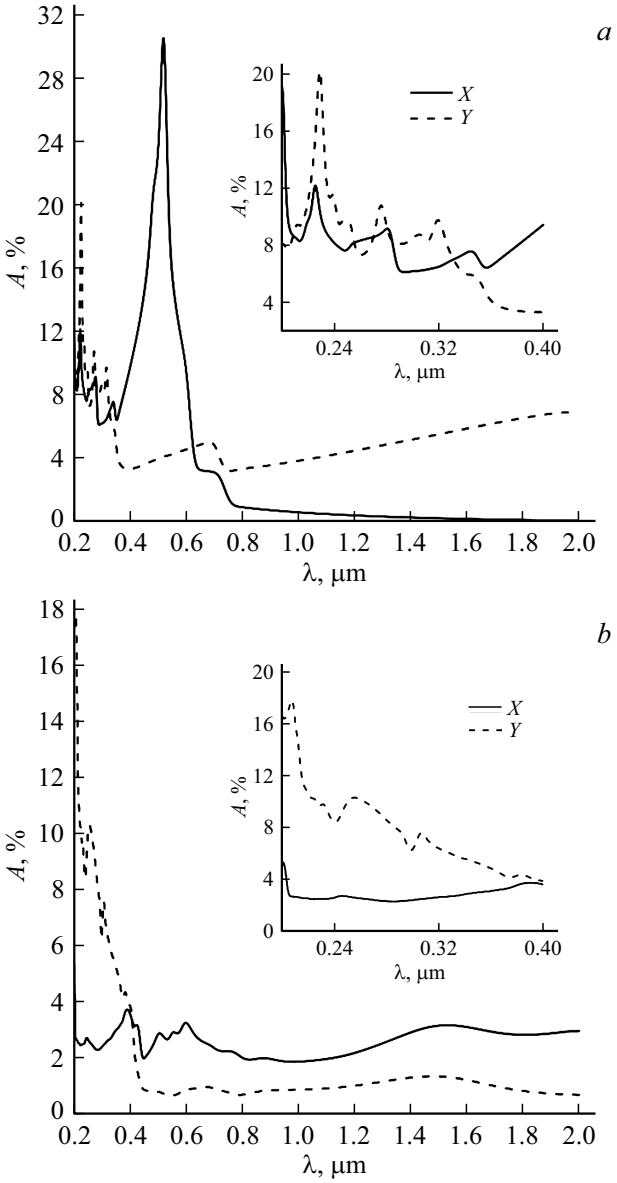

Figure 4. Optical absorption coefficient of the van der Waals borophene/ZnO heterostructure with light polarized along the X (solid curves) and Y (dashed curves) axes: a — with oxidized borophene; b — with pure borophene.

Optical and optoelectronic properties of van der Waals heterostructures based on oxidized borophene

The optical and optoelectronic properties of the examined van der Waals heterostructures were analyzed based on the calculated absorption spectra and photocurrent spectra within the $0.2-2\,\mu$m wavelength range. The calculated absorption spectra for O-borophene/GaN and O-borophene/ZnO heterostructures are presented in Figs. 3 and 4, respectively. The cases of light polarization along the X axis (perpendicular to the zigzag edge of O-borophene) and the Y axis (along the zigzag edge of O-borophene) were considered. Absorption spectra of the same heterostructures with non-functionalized borophene were also calculated (see Figs. 3 and 4) in order to establish the influence of functionalization of borophene with oxygen on the patterns of absorption of electromagnetic radiation by the studied van der Waals heterostructures. These plots demonstrate clearly that the oxidation of borophene changed radically the profile of the absorption spectrum of borophene/GaN and borophene/ZnO heterostructures when light was polarized along axis X. An absorption peak emerged in this case in the visible region with an intensity that was the maximum one for these heterostructures (approximately 30%). With no oxygen functional-

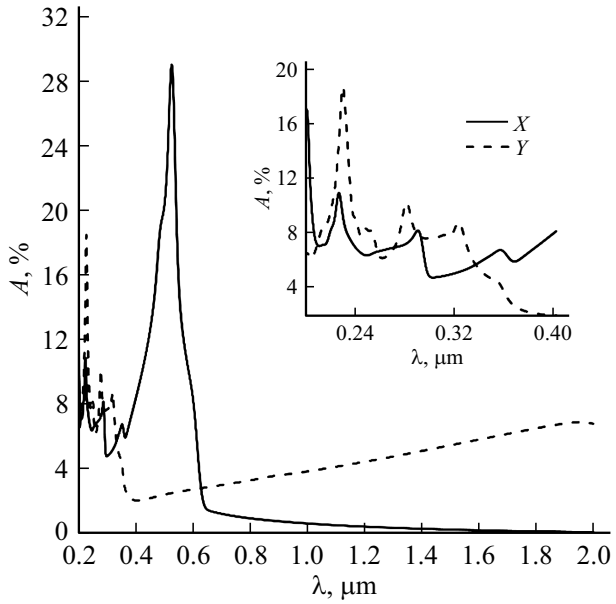

Figure 5. Optical absorption coefficient of oxidized borophene with light polarized along the X (solid curves) and Y (dashed curves) axes.

ization of borophene, the absorption for borophene/GaN and borophene/ZnO heterostructures remained below ~ 10 and $\sim 5\%$, respectively, within the entire examined wavelength range. When waves are polarized along the Y axis, the profiles of absorption spectra of borophene/GaN and borophene/ZnO heterostructures with oxidized and non-oxidized borophene are almost identical.

The reason for such noticeable changes in the absorption spectrum of O-borophene/GaN and O-borophene/ZnO heterostructures occurring when light is polarized along the X axis lies in the topology of O-borophene. Figure 1 shows clearly that „bridges“ of covalent bonds between an oxygen atom and neighboring boron atoms in borophene extend along the X axis. Thus, the functionalization of borophene with oxygen is most noticeable in the direction of axis X. The absorption spectra of oxidized borophene corresponding to two directions of light polarization shown in Fig. 5 verify the validity of this claim. The presented plot features an absorption peak with intensity $\sim 30\%$ in the visible range that is exactly the same as the peak found in the absorption spectra of van der Waals O-borophene/GaN and O-borophene/ZnO heterostructures when light is polarized along the X axis.

Photocurrent spectra were calculated based on the obtained absorption spectra and solar radiation spectra on the surface of the Earth' (AM1.5) and outside the Earth's atmosphere (AM0). AM0 and AM1.5 solar radiation spectra were taken from the National Renewable Energy Laboratory [38] website that lists solar spectra data in the $280-2000$ nm wavelength range. The calculated photocurrent spectra of O-borophene and van der Waals heterostructures based on it are shown in Fig. 6. The presented photocurrent values correspond to a surface area of $1\,\text{cm}^2$. The photocurrent peak for O-borophene is located in the visible region at a wavelength of $0.531\,\mu$m, and its height is $13.42\,\text{mA}\cdot\text{cm}^{-2}\cdot\mu\text{m}^{-1}$ under AM0 conditions and $10.96\,\text{mA}\cdot\text{cm}^{-2}\cdot\mu\text{m}^{-1}$ under AM1.5 conditions. The photocurrent increases within the wavelength range from ~ 0.4 to $\sim 0.65\,\mu$m, which covers more than one half (62.5%) of the visible radiation spectrum ($0.38-0.78\,\mu$m). Here and elsewhere, the atmosphere causes dips in the photocurrent in the IR region due to absorption of electromagnetic radiation with its wavelengths falling within the corresponding range. The photocurrent spectra of O-borophene/GaN and O-borophene/ZnO heterostructures are similar in shape to the spectra of O-borophene. The height of the photocurrent peak at a wavelength of $0.561\,\mu$m for the O-borophene/GaN heterostructure is $14.97\,\text{mA}\cdot\text{cm}^{-2}\cdot\mu\text{m}^{-1}$ under AM0 conditions and $12.36\,\text{mA}\cdot\text{cm}^{-2}\cdot\mu\text{m}^{-1}$ under AM1.5 conditions. The height of the photocurrent peak (at a wavelength of $0.524\,\mu$m) for the O-borophene/ZnO heterostructure is 14.22 and $11.61\,\text{mA}\cdot\text{cm}^{-2}\cdot\mu\text{m}^{-1}$ under AM0 and AM1.5 conditions, respectively.

The integral photocurrent (or photocurrent density) is one of the key characteristics of photovoltaic devices. The calculated values of integral photocurrent for the entire solar radiation spectrum and the visible range of the solar spectrum ($380-780$ nm) and the maximum photocurrent values at a wavelength of 550 nm, which corresponds to the maximum solar radiation power, are listed in the table. It follows from these data that the functionalization of borophene with oxygen leads to a twofold increase in the integral photocurrent of the borophene/GaN and borophene/ZnO heterostructures for the AM0 and AM1.5 spectra. In the visible range, the integral photocurrent for heterostructures with O-borophene is several times higher than the integral photocurrent of heterostructures with non-functionalized borophene. The maximum photocurrent at a wavelength of 550 nm increases by a factor of 6 for the O-borophene/GaN and O-borophene/ZnO heterostructures. It should also be noted that the integral photocurrent of the O-borophene/GaN and O-borophene/ZnO heterostructures in the visible range correlates well with its values for the graphene/MoS_2 heterostructure ($\sim 3\,\text{mA/cm}^2$) [39] and multilayer WS_2 ($4.10\,\text{mA/cm}^2$) determined in an actual experiment [40].

Conclusion

The following conclusions may be inferred from the results of the study. Functionalization of borophene with oxygen with the formation of covalent bonds on one side of a borophene monolayer opens up a gap in the band structure of van der Waals borophene/GaN (gap width, 0.13 eV) and borophene/ZnO heterostructures (0.22 eV). Owing to the semiconductor type of conductivity, a characteristic high-intensity peak emerges in the optical absorption

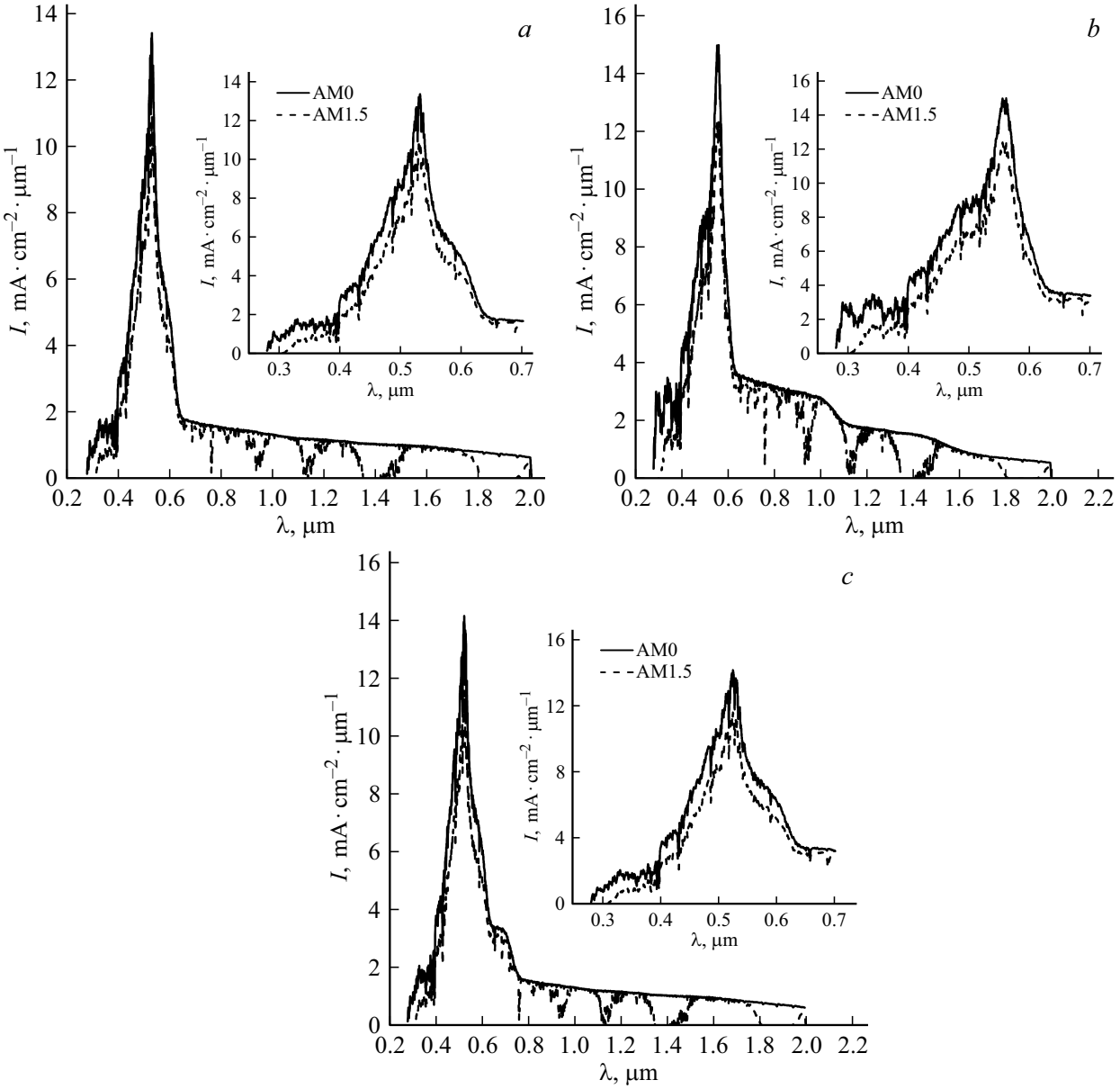

Figure 6. Spectra of photocurrent on the surface of the Earth (AM1.5, dashed curves) and outside the Earth's atmosphere (AM0, solid curves): *a* — for a monolayer of oxidized borophene; *b* — for a van der Waals heterostructure based on oxidized borophene and GaN; and *c* — for a van der Waals heterostructure based on oxidized borophene and ZnO.

and photocurrent spectra of O-borophene/GaN and O-borophene/ZnO heterostructures in the visible range. This is important for efficient operation of solar cells based on these structures. The presence of oxidized borophene in the examined heterostructures leads to a six-fold increase in the maximum photocurrent (compared to the parameters of heterostructures with pure borophene) at a wavelength of 550 nm. Therefore, oxygen functionalization allows one to control the location and intensity of the optical absorption and photocurrent peaks of borophene-based heterostructures. It is predicted that van der Waals O-borophene/GaN and O-borophene/ZnO heterostructures may be promising as sensitive elements of solar cells operating both on the Earth's surface and beyond. This notion is corroborated by a fine agreement with the results of experiments with other layered vertical 2D structures.

Funding

This work was supported by a grant from the Russian Science Foundation (project No. 21-72-00082, https://rscf.ru/project/21-72-00082/).

Conflict of interest

The authors declare that they have no conflict of interest.

Optoelectronic characteristics of the studied van der Waals heterostructures

Structure	Integral photocurrent for the entire solar radiation spectrum, mA/cm^2	Photocurrent maximum at a wavelength of 550 nm, mA·cm^{-2} · μm^{-1}	Integral photocurrent for the visible 380−80 nm range, mA/cm^2
Solar spectrum AM0			
O-borophene/GaN	4.59	13.81	2.40
O-borophene/ZnO	3.66	8.54	2.37
O-borophene	3.20	7.94	1.92
borophene/GaN	2.08	2.76	1.20
borophene/ZnO	1.51	1.46	0.64
Solar spectrum AM1.5			
O-borophene/GaN	3.42	11.42	1.95
O-borophene/ZnO	2.73	7.06	1.87
O-borophene	2.36	6.57	1.50
borophene/GaN	1.49	2.28	0.92
borophene/ZnO	1.07	1.21	0.46

References

[1] P. Ares, K.S. Novoselov. Nano Mater. Sci., **4**, 3 (2021). DOI: 10.1016/j.nanoms.2021.05.002

[2] J. Azadmanjiri, V.K. Srivastava, P. Kumar, Z. Sofer, J. Min. J. Gong. Appl. Mater. Today, **19**, 100600 (2020). DOI: 10.1016/j.apmt.2020.100600

[3] X. Zhou, E.E. Rodriguez. Chem. Mater., **29**, 5737 (2017). DOI: 10.1021/acs.chemmater.7b01561

[4] R. Lv, J.A. Robinson, R.E. Schaak, D. Sun, Y. Sun, T.E. Mallouk, M. Terrones. Acc. Chem. Res., **48**, 56 (2015). DOI: 10.1021/ar5002846

[5] G. Murali, J.K. Reddy Modigunta, Y.H. Park, J.H. Lee, J. Rawal, S.Y. Lee, I. In, S.J. Park. ACS Nano, **16**, 13370 (2022). DOI: 10.1021/acsnano.2c04750

[6] L. Li, Y. He, L. Xu, H. Wang. Appl. Sci., **9**, 5211 (2019). DOI: 10.3390/app9235211

[7] H. Xie, Z. Li, L. Cheng, A.A. Haidry, J. Tao, Y. Xu, K. Xu, J. Z. Ou. iScience, **25**, 103598 (2022). DOI: 10.1016/j.isci.2021.103598

[8] M.C. Wang, C.C. Huang, C.H. Cheung, C.Y. Chen, S.G. Tan, T.W. Huang, Y. Zhao, Y. Zhao, G. Wu, Y.P. Feng, H. Wu, C. Chang. Ann. Der Phys., **532**, 1900452 (2020). DOI: 10.1002/andp.201900452

[9] A.K. Geim, I.V. Grigorieva. Nature, **499**, 419 (2013). DOI: 10.1038/nature12385

[10] K.S. Novoselov, A. Mishchenko, A. Carvalho, A.H. Castro Neto. Science, **353**, aac9439 (2016). DOI: 10.1126/science.aac94

[11] A. Di Bartolomeo. Nanomaterials, **10**, 579 (2020). DOI: 10.3390/nano10030579

[12] J. Yao, G. Yanga. J. Appl. Phys., **131**, 161101 (2022). DOI: 10.1063/5.0087503

[13] Z. Wang, B. Xu, S. Pei, J. Zhu, T. Wen, C. Jiao, J. Li, M. Zhang, J. Xia. Sci. China Inf. Sci., **65**, 211401 (2022). DOI: 10.1007/s11432-021-3432-6

[14] Z.U.D. Babar, A. Raza, A. Cassinese, V. Iannotti. Molecules, **28**, 2275 (2023). DOI: 10.3390/molecules28052275

[15] S.K. Chakraborty, B. Kundu, B. Nayak, S.P. Dash, P.K. Sahoo. iScience, **25**, 103942 (2022). DOI: 10.1016/j.isci.2022.103942

[16] X. Zhou, X. Hu, J. Yu, S. Liu, Z. Shu, Q. Zhang, H. Li, Y. Ma, H. Xu, T. Zhai. Adv. Funct. Mater., **28**, 1706587 (2018). DOI: 10.1002/adfm.201706587

[17] S. Liang, B. Cheng, X. Cui, F. Miao. Adv. Mater., **32**, 1903800 (2020). DOI: 10.1002/adma.201903800

[18] Q. Tang, F. Zhong, Q. Li, J. Weng, J. Li, H. Lu, H. Wu, S. Liu, J. Wang, K. Deng, Y. Xiao, Z. Wang, T. He. Nanomaterials, **13**, 1169 (2023). DOI: 10.3390/nano13071169

[19] P. Lin, J.K. Yang. J. Alloys Compd., **842**, 155890 (2020). DOI: 10.1016/j.jallcom.2020.155890

[20] N. Shehzad, S. Saeed, I. Shahid, I. Khan, I. Saeed, J.A. Zapien, L. Zhang. RSC Adv., **12**, 31456 (2022). DOI: 10.1039/D2RA03439E

[21] Y.V. Kaneti, D.P. Benu, X. Xu, B. Yuliarto, Y. Yamauchi, D. Golberg. Chem. Rev., **122**, 1000 (2022). DOI: 10.1021/acs.chemrev.1c00233

[22] X. Liu, M.C. Hersam. Sci. Adv., **5**, eaax6444 (2019). DOI: 10.1126/sciadv.aax644

[23] L. Li, J.F. Schultz, S. Mahapatra, X. Liu, C. Shaw, X. Zhang, M.C. Hersam, N. Jiang. J. Am. Chem. Soc., **143**, 15624 (2021). DOI: 10.1021/jacs.1c04380

[24] R. Abbasi, R. Faez, A. Horri, M.K. Moravvej-Farshi. J. Appl. Phys., **132**, 034302 (2022). DOI: 10.1063/5.0092647

[25] N. Katoch, A. Kumar, R. Sharma, P.K. Ahluwalia, J. Kumar. Phys. E: Low-Dimens. Syst. Nanostructures, **120**, 113842 (2020). DOI: 10.1016/j.physe.2019.113842

[26] S. Jing, W. Chen, J. Pan, W. Li, B. Bian, B. Liao, G. Wang. Mater. Sci. Semicond. Process., **146**, 106673 (2022). DOI: 10.1016/j.mssp.2022.106673

[27] J.W. Jiang, X.C. Wang, Y. Song, W.B. Mi. Appl. Surf. Sci., **440**, 42 (2018). DOI: 10.1016/j.apsusc.2018.01.140

[28] M.M. Slepchenkov, D.A. Kolosov, O.E. Glukhova. Materials, **15**, 4084 (2022). DOI: 10.3390/ma15124084

[29] J.P. Perdew, J.A. Chevary, S.H. Vosko, K.A. Jackson, M.R. Pederson, D.J. Singh, C. Fiolhais. Phys. Rev. B, **46**, 6671 (1992). DOI: 10.1103/PhysRevB.46.6671

[30] J.M. Soler, E. Artacho, J.D. Gale, A. García, J. Junquera, P. Ordejón, D. Sánchez-Portal. J. Phys.: Condens. Matt., **14**, 2745 (2002). DOI: 10.1088/0953-8984/14/11/302
[31] S. Grimme. J. Comput. Chem., **27**, 1787 (2006). DOI: 10.1002/jcc.20495
[32] P. Pulay. Chem. Phys. Lett., **73**, 393 (1980). DOI: 10.1016/0009-2614(80)80396-4
[33] H.J. Monkhorst, J.D. Pack. Phys. Rev. B, **13**, 5188 (1976). DOI: 10.1103/PhysRevB.13.5188
[34] S.L. Dudarev, G.A. Botton, S.Y. Savrasov, C.J. Humphreys, A.P. Sutton. Phys. Rev. B, **57**, 1505 (1998). DOI: 10.1103/PhysRevB.57.1505
[35] E.N. Economou. *Green's Functions in Quantum Physics*, 3rd ed. (Springer, Berlin, 1983), p. 55–75. DOI: 10.1007/3-540-28841-4_4
[36] Y. He, N. Cheng, C. Chen, S.Y. Xiong, J.W. Zhao. Sci. China Technol. Sci., **62**, 799 (2019). DOI: 10.1007/s11431-018-9385-x
[37] X. Liu, M.S. Rahn, Q. Ruan, B.I. Yakobson, M.C. Hersam. Nanotechnology, **33**, 10 (2022). DOI: 10.1088/1361-6528/ac56bd
[38] *National Renewable Energy Laboratory* (*NREL*). [Electronic source]. URL: https://www.nrel.gov/.
[39] D.B. Seo, T.N. Trung, S.S. Bae, E.T. Kim. Nanomaterials, **11**, 1585 (2021). DOI: 10.3390/nano11061585
[40] C.M. Went, J. Wong, P.R. Jahelka, M. Kelzenberg, S. Biswas, M.S. Hunt, A. Carbone, H.A. Atwater. Sci. Adv., **5**, eaax6061 (2019). DOI: 10.1126/sciadv.aax60

Translated by D.Safin